

Development of Space-to-Ground Radio Interference Forecasting Software and a X-Ku (10.7-12.7GHz) band RFI Monitor

Artem Davydov*

Department of Physics and Astronomy, University of British Columbia
6224 Agricultural Road, Vancouver, British Columbia, Canada, V6T 1Z1

(Dated: November 23, 2021)

The unprecedented increase of communication satellites (ComSats) in low earth orbit (LEO) presents a new challenge to radio astronomers. We propose to characterize the expected radio emission from ComSats in the Ku band using a combination of emission prediction simulations and an in-band radio survey at the Dominion Radio Astronomy Observatory (DRAO). We are currently developing a 4GHz digital acquisition system to be complemented with a T.V. satellite dish and an Low Noise Block (LNB) to be welded on the DRAO site. The mapping of radio interference in the X-Ku (10.7-12.7GHz) band will directly translate to digital system design requirements of the novel Canadian Galactic Emission Mapper (CGEM) telescope. The survey will also contribute to the growing body of research into the impact of ComSats on astronomy.

PACS numbers:

I. MOTIVATION

The advancement of telecommunication technologies was driven by the development of the theory of electromagnetism and accelerated by the necessity for fast communication over long distances imposed by war time[3]. A typical trench radio from world war 1 is shown in the figure 1.



FIG. 1: Three US soldiers gathered around a receiving trench radio. Set ups like these were used to transfer intelligence to and from the battlefield during war time. The ability to quickly send orders and transfer intelligence determined the course of the war. The same technology is widely used today for telecommunications. (Credit: Illinois Digital Heritage Hub)

The microwave frequency range represents a limited portion of the electromagnetic spectrum that is not absorbed by the atmosphere. This makes the microwave frequency a natural choice for telecommunication operators and many earth based astronomical observations. An explanatory diagram is shown in figure 2.

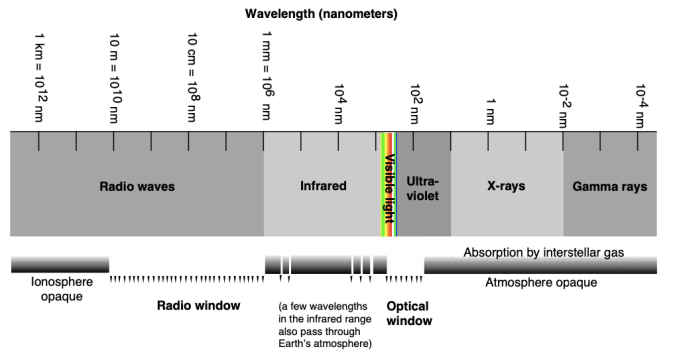


FIG. 2: A cartoon of the atmospheric window of electromagnetic radiation. The top horizontal ruler provides a scale of the wavelengths of electromagnetic radiation in nanometers, increasing to the left. Note that the two largest gaps with no significant absorption coincide with the visible (650-1200nm) and radio wavelengths(approximately 1cm-10m). These are indicated by gaps in the bottom bar of the figure. The majority of the spectrum is opaque to our atmosphere. (Credit: NASA Radio JOVE Project)

Electromagnetism is a wave like phenomena. The principle of superposition dictates that if we were to measure the electromagnetic field at any point in space, we would be measuring the contribution from all source of radiation passing through the point in that time. The measured signal is simple the sum of all electromagnetic radiation passing through that point. Radio astronomical apparatus is designed to measure radio signals received from the sky which are characteristically orders of magnitude less relative to artificial sources of radiation such as cell-phone towers or television satellites. A radio receiver

*Electronic address: artiumdav@student.ubc.ca

integrated into a telescope is susceptible to interference from telecommunication satellites due to the sharing of a common band. In the last decade multiple companies received authorization by the FCC to launch satellite constellation to provide global internet[4][5][6]. These constellations range in size between dozens to hundreds per orbital planes and elevation angle. Each of these satellites communicates with the customer and its ground station in the X-Ku band (10.7-12.7GHz). Radiation from an ensemble of these satellites can potentially swamp significant astrophysical signals. Such effects can be mitigated by the telescope designers but this requires an understanding of the expected radio background on site. Some of the satellites used by operators are capable of modulating the radiation flux they transmit to the surface of the earth [7]. The potential impact of SatCom constellations on astronomy was felt by optical astronomers in November 2019. The Cerro Tololo Inter-American Observatory (CTIO) released photos from a 333 seconds-exposure where at least 19 bright streaks are visible. The streaks are attributed to reflections off of a "train" of StarLink satellites[2]. The photograph is shown in figure 3. The StarLink constellation's down-link frequency coincides with the receiver frequency on the Square Kilometer Array (SKA) Mid telescope located in South Africa. An analysis performed by the SKA organization predicts that for a constellation of significantly large size (100,000 satellites) potentially threatens the viability of their entire observation band[1].Cooperation between operators and astronomers will be of utmost importance in the scenario where large portions of the microwave band is saturated by telecommunication signals.

The Experimental Cosmology Group at University of British Columbia is currently working on a new radio telescope. The Canadian Galactic Emission Mapper (CGEM) telescope will observe the 8-10GHz polarized sky. The frequency was chosen to target the Galactic synchrotron emission. The frequency band of CGEM is adjacent to the down link band of the SpaceX Starlink constellation (10.7-12.7 GHz). We will develop a computer simulation that models the position of each deployed satellite for a given observation time windows (ephemeris data). This will be used to produce forecasts for the presence of satellite within the telescope line of sight. Using the position and expected radio emission level from satellites we will derive an estimated power level intercepted by our dish during the observation window. We will also develop a 4GHz digital acquisition system that we will connect to an analog front end. The analog front end will be built using cheaply available over the counter TV dish and a low noise block. The Radio Frequency Interference (RFI) monitor will be wielded at the DRAO site to measure the power intercepted from the sky at 3 different pointings. The severity of radio contamination can be derived from the spectrum of the measurement. RFI expectations derived from our observations will be utilized by the group to inform the digital system design of CGEM. The code used to simulate the

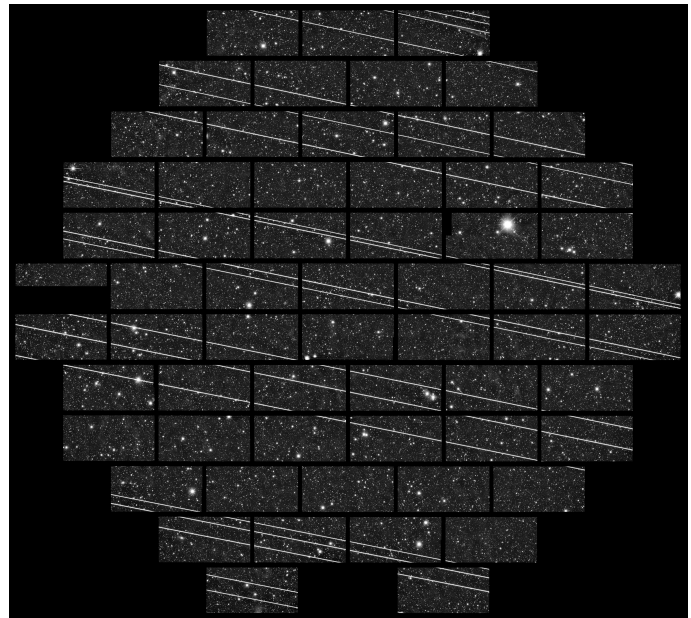


FIG. 3: A photo from a 333 second exposure taken by DECam on the Blanco 4-meter telescope at the Cerro Tololo Inter-American Observatory (CTIO). The streaks correspond to satellites of the StarLink constellation. Pixels with light contamination from these satellites lose viability deeming them unusable for inference of astrophysical information. (Credit: NOIRlab)

ephemeris data and expected power levels will be made widely available to the community. The development of the digital back end will be documented and the characterization of the Analog-to-Digital (ADC) converter will be made available to other experimenters and the community as well. Lastly, this project will contribute to the community's understanding of the changing radio sky.

II. THEORY

A. Radio Interference Monitor

1. Analog Domain

To measure the radio signal at the DRAO site we need to construct a receiver antenna sensitive to radiation in the X-Ku band. The idealized dipole antenna can be used to illustrate the design decisions and theory we have to consider. An oscillating electric field produces a current across the dipole antenna depicted in figure 4.

The energy emitted by a source is expressed in terms of flux density (F) and are measured in Watts per meters squared (W/m^2). The energy intercepted by a dish is therefore:

$$P(t) = \vec{A}(t) \cdot \vec{F}(t) \quad (1)$$

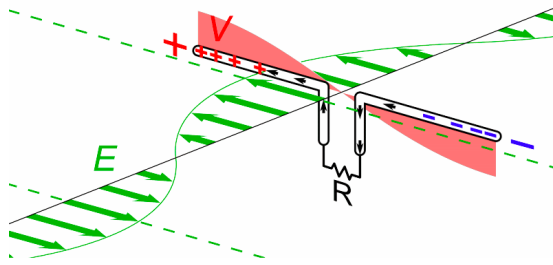


FIG. 4: A snap shot of an electric field, E , depicted as green arrows enveloped by oscillating line passing through a dipole antenna. The changing electric field carried by the electromagnetic wave induces a current (black arrows along the antenna) by moving the free charges in the antenna. A resistor, R , connects the two conducting wires comprising the antenna. A measurable voltage V (filled red curve perpendicular to E field plane) is dropped across the resistor. (Credit: Chetvorno, CC0, via Wikimedia Commons)

Where \vec{A} points in the direction normal to the surface containing the dish rim. The length of the vector is the effective area of the dish $A = \pi(D/2)^2$ for a dish width diameter D . The vector \vec{F} points the direction of the pointing vector and its magnitude is the flux density arriving from the source. Lastly, the resultant dot product $P(t)$ encodes the electromagnetic energy intercepted by the dish.

Let us denote the voltage dropped across the resistor R with:

$$V(t) = V_{sky}(t) + V_{interference}(t) + V_{noise}(t) \quad (2)$$

The voltage measured includes the contribution of all source including the wanted sky signal and the unwanted system noise and external interference. The sky signal is expected to be faint therefore a low noise amplifier with gain G_{RF} is required for successful detection. We are interested in a limited bandwidth that will be then digitized. This requires the introduction of a band-pass filter. The band-pass filter can be mathematically represented in the frequency domain using Heaviside functions:

$$F_{bp} = U(\nu - \nu_{up}) - U(\nu_{lo}) \quad (3)$$

The output voltage after the band pass is:

$$V_{bp} = \mathfrak{F}^{-1}(\mathfrak{F}(V_{RF}(t)G_{RF})F_{bp}) \quad (4)$$

Low noise amplifiers with sufficient gain for high frequency signals are expensive. The band limited, high frequency signal is "copied" down to a lower frequency using a mixer. A mixer is a circuit component that multiplies an input signal coming in at a frequency (RF) with a sine wave with an intermediate frequency (IF) and outputs a signal that contains the sums and differences of

the frequencies. In the case of a pure harmonic (ν_{RF}) input signal the mixer acts as follows [8]:

$$\begin{aligned} V_{bp}(t)\sin(2\pi\nu_{IF}t) = \\ \cos[2\pi(\nu_{IF} - \nu_{RF})t] - \cos[2\pi(\nu_{RF} + \nu_{IF})t] \end{aligned}$$

Where $V_{bp}(t) = 2\sin(2\pi\nu_{RF}t)$, and the mixed down component is given by:

$$V_{IF}(t) = \cos[2\pi(\nu_{IF} - \nu_{RF})t] \quad (5)$$

The higher frequency ($\nu_{RF} + \nu_{IF}$) component can be filtered with a low pass filter represented in the frequency domain gain using a Heaviside function:

$$F_{lp} = 1 - U(\nu_{cut}) \quad (6)$$

Where ν_{cut} is chosen such that the higher frequency component is filtered without losing any of the lower frequency copy at $(\nu_{RF} - \nu_{IF})$. The low frequency signal can now be amplified using cheaper hardware with gain G_{IF} . Finally, the output voltage of the system is given by:

$$V_{bp}(t) = \mathfrak{F}^{-1}(\mathfrak{F}(V_{IF}(t)G_{IF})F_{lp}) \quad (7)$$

The output of the cascaded electrical circuit consisting of the antenna, low noise high frequency amplifier, band pass filter, mixer, low pass filer, and finally the intermediate frequency amplifier is fed to an Analog-to-Digital converter. A flow chart is shown in figure 5. The theory behind successful digitization of a discretely sampled analog signal is covered next.

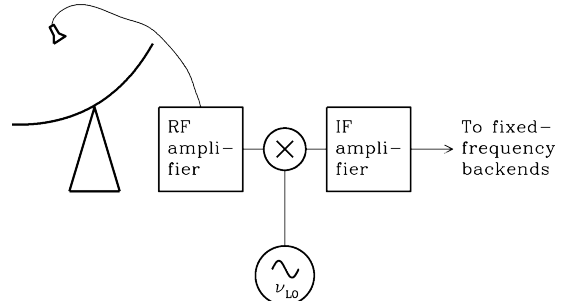


FIG. 5: A flow chart cartoon of a radio telescope. The radio dish on the left most of the diagram feeds the receiver dangling above it. The receiver is connected to an RF amplifier. The amplifier output to a mixer with a local oscillator operating at a frequency of ν_{lo} . The mixer outputs to an intermediate frequency amplifier that is connected to a fixed frequency back-end (right most of the diagram). (Credit: NRAO)

2. Digital Domain

The Nyquist-Shannon condition sets a lower limit on the sampling frequency for which the analog signal can be reliably reconstructed. The Nyquist-Shannon inequality for the case of a band limited input signal we have:

$$T < \frac{1}{2\nu_c} \quad (8)$$

We derive a lower sampling frequency requirement for our digital acquisition systems ADC from the above inequality. The expected bandwidth of the CGEM experiment is 2GHz. The bandwidth that will be sampled using our RFI monitor is 1GHz. This sets a sliding scale requirement for an ADC sampling frequency of 2-4GHz. A system capable of managing sampling at this frequency, processing and saving the data is realizable using available FPGA technology.

B. Kepler's Equation

To model the position of satellites at any given time it is necessary to solve Kepler's equation. Kepler's equation encapsulates the position of an object in polar coordinates at some time with respect to a reference initial time:

$$M = E - e \sin(E) \quad (9)$$

Where M is the mean anomaly, e is the eccentricity of the orbit, and E is the eccentric anomaly. The equation cannot be inverted to solve for the position at time t as it is transcendental. Numerical methods exist to solve for the position of an object in the orbital plane. These three parameters are not sufficient to recover the 3D position vector of the object. The orbital plane can be both inclined and rotated with respect to the stationary earth. The inclination (i) of the orbital plane, right ascension of the ascending node (Ω), and the argument of perigee (ω) need to be added for a complete parametrization of the 3D orbit with respect to a stationary earth frame of reference. An illustration of a generic earth-centric orbit with labeled orbital parameters is depicted in figure 6.

III. DETAILS ON PROPOSED EXPERIMENT/CALCULATION

A. Simulations

We will simulate the orbits of major communication satellite constellations. The North American Aerospace Defense Command (NORAD) publishes the orbital parameters necessary to simulate the position and velocity of the satellites as a function of time. The data

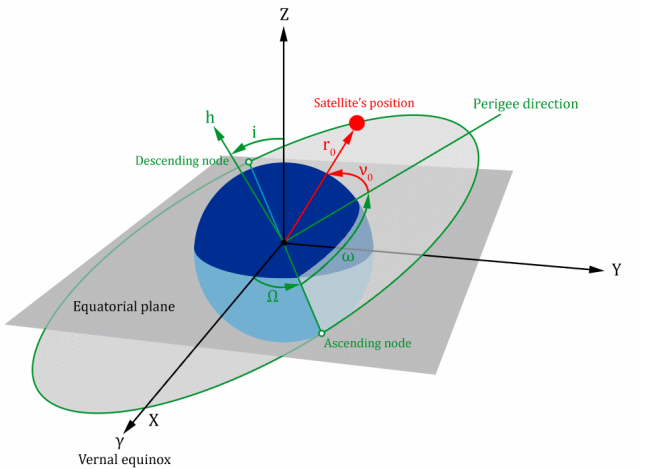


FIG. 6: A depiction of a generic Keplerian orbit defined with respect to an earth stationary frame. The earth stationary frame has the X axis pointing in the direction of the Vernal Equinox, the Z axis points in the direction of the celestial pole, and Y is chosen to complete a right handed coordinate system. The quantities r_0 and v_0 correspond to the velocity and position of the satellite with respect to the orbital plane. The orbital plane contains the green ellipse. Ω is the angle between the vernal equinox and the ascending node vector in the XY plane. The argument of perigee ω is the angle subtended between the ascending node and the perigee direction. The descending node, h , is the vector normal to the orbital plane and the orbital inclination, i , is the angle between h and the Z axis. (Credit: MATLAB Central File Exchange)

is available in Two Line Element format (TLE) on the CelesTrak website (<https://celestak.com>). The data is updated on a regular basis normally refreshing every 24 hours. The Simplified General Perturbations (SGP4) is an algorithm that was published to solve for the ephemeris of object in Keplerian orbits. SGP4 incorporates the effects of earth's gravitation, the moon's gravitational field, and atmospheric drag [9]. Simulated telescope pointing will be written in python. The script will calculate the location of a every satellite with respect to the bore-sight at every time step of a simulated observation time window. A depiction of 100 StarLink orbit traces produced by our simulator is illustrated in figure 7.

The expected flux density at earth from StarLink satellites is provided in SpaceX's Power Flux Density FCC filing [10]. The expected flux densities will be used to calculate the power intercepted by our dish at any given time during the observation window. This will set an upper limit on the expected interference from a typical SatCom constellation. An example duty cycle produced by our script is shown in figure 8.

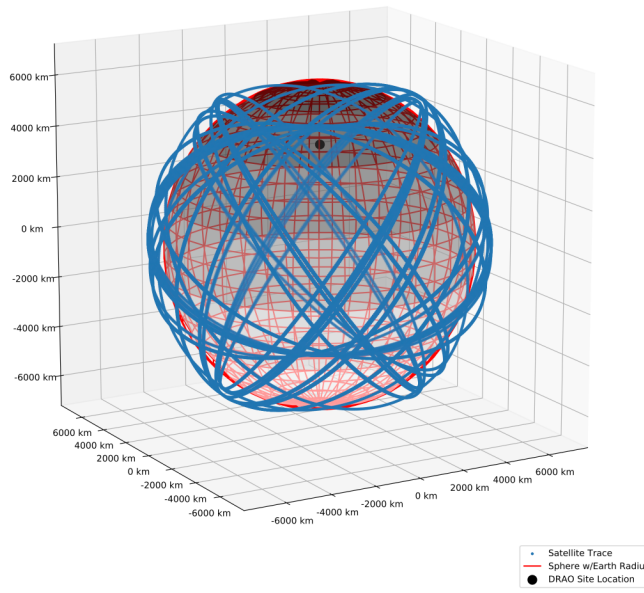


FIG. 7: A 30 minute orbit trace of 100 StarLink satellites produced from state vectors calculated using TLEs from NORAD and the SGP4 algorithm. The simulated observation takes place on October 30th, 2021 between 12:30:30pm - 13:30:31pm using the StarLink satellite TLE data set of October 29th. The traces drawn in blue are comprised of positions of the satellites separated by 10 seconds. The black dot marks the position of the DRAO site on the sphere with the radius of the earth (6300Km). The red wire frame denotes the surface of the earth. (Credit: Artem Davydov)

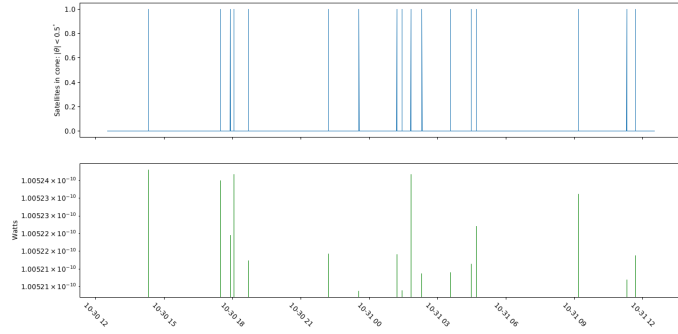


FIG. 8: The top plot's vertical axis enumerates the count of satellites within 0.5 degrees of the bore sight. The vertical axis of the bottom plot is the sum contribution of the incoming flux within the 0.5 degrees cone calculated using equation (1). The horizontal axis measures the time of observation and is shared between the top and bottom plots. (Credit: Artem Davydov)

B. Radio Interference Monitor

The analog front end will be built using a satellite TV dish and a Low Noise Block. A block diagram depicting the high level design of the RFI monitor is shown in figure xx.xx. The dish used is an off-axis, 33 inch diameter, parabolic reflector with a housing for an Low

Noise Block. A Low Noise Block contains a feed horn and an antenna. We used the SatMaximum Universal Single LNB (SM 2010-01) with an integral feed horn and a standard 40mm neck. These LNBs are designed for satellite television receiver dishes and are normally connected to a TV box which mixes down the signal to an intermediate frequency and then decoded. To utilize the LNB in the absence of a TV box we introduce a bias tee between the LNB and the ADC acquisition system. The LNB accepts two settings inputs: a DC current level of 13V or 18V to switch between horizontal and linear polarization setting respectively. The local oscillator frequency is controlled by an input tone of 0KHz or 22KHz corresponding to a local oscillator frequency of 9.75GHz or 10.6GHz respectively. We will feed the LNB with a 13V DC signal with no tone corresponding to the LNB being set to measure horizontal polarization and the local oscillator value set to 9.75GHz. The output of the bias tee is fed to the ADC on the Xilinx ZCU111 evaluation board. The ADC set to sample the signal at 4GSPS in 8 microsecond bursts. The ADC was programmed by Parham Zarei of the UBC Experimental Cosmology group. We will commit the ADC output to memory for post analysis of the spectrum and time series data. A block diagram of our design is shown in figure 9.

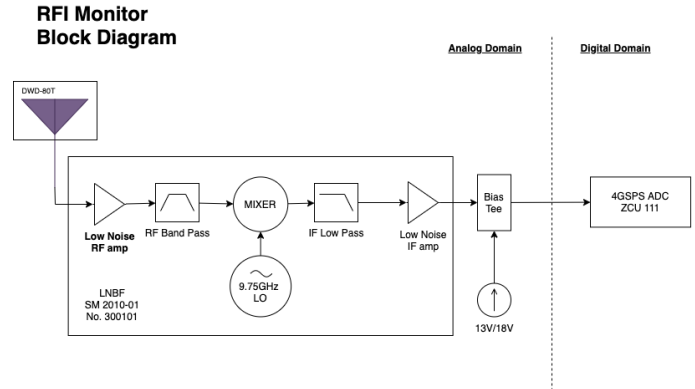


FIG. 9: A flow chart of the RFI monitor. The chart is separated by a vertical dashed line indicating the transition from the analog domain on the left to the digital domain on the right. The DWD-80T dish (upper left) will launch radiation into the feed horn of SM 2010-01 LNB. The LNB will amplify the RF signal, band-pass it, mix it with an IF signal, filter out the higher frequency mixed signal, and finally amplify the resultant IF signal. The cascaded circuit is shown as a large rectangular block. The output IF signal is fed to a bias tee that routes the output to the Xilinx ZCU111 ADC in the digital domain. The bias tee also feeds the polarisation control voltage (13V or 18V) to the LNB. (Credit: Artem Davydov)

IV. RESOURCES LIST

The Xilinx ZCU111 evaluation kit was already acquired by the UBC Experimental Cosmology group. The

DWD-80T TV dish and SM2020-01 LNB were purchased by the group and are ready for assembly. A suitable bias tee was identified and it will be sourced by the group. The necessary computing resources are also available at the laboratory. The simulator relies strictly on open source software (SGP4) that is freely available for download.

V. PLANNED SCHEDULE

A tentative action plan:

1. **Programming the ADC to Ethernet down-link:** December
2. **Constructing the Dish, LNB, Bias Tee:** January
3. **First site Survey:** January-February
4. **Data analysis:** February-March
5. **Thesis writing:** March-April

- [1] "Skao Needs Corrective Measures from Satellite 'Mega-Constellation' Operators to Minimise Impact on Its Telescopes." Public Website, 7 Oct. 2020, <https://www.skatelescope.org/news/skao-satellite-impact-analysis/>.
- [2] Info@noirlab.edu. "Starlink Satellites Imaged from CTIO." <https://noirlab.edu/public/images/iotw1946a/>.
- [3] "Golden Age of Radio in the US." Radio on the Frontlines: WWI and WWII — DPLA, <https://dp.la/exhibitions/radio-golden-age/radio-frontlines>.
- [4] "WorldVu Satellites Limited, Debtor-in-Possession, Petition for Declaratory Ruling Granting Access to the U.S. Market for the OneWeb Non-Geostationary Satellite Orbit Fixed-Satellite Service V-Band System", Aug 26, 2020, <https://www.fcc.gov/document/fcc-grants-oneweb-us-market-access-expanded-ngso-constellation>
- [5] "FCC Authorizes SpaceX to Provide Broadband Satellite Services", Mar 29, 2018, <https://www.fcc.gov/document/fcc-authorizes-spacex-provide-broadband-satellite-services>
- [6] "FCC Authorizes Kuiper Satellite Constellation", Jul 30, 2020, <https://www.fcc.gov/document/fcc-authorizes-kuiper-satellite-constellation>
- [7] "Application for Fixed Satellite Service by Space Exploration Holdings, LLC", March 29, 2018, <https://fcc.report/IBFS/SAT-LOA-20161115-00118>
- [8] Chapter 3 Radio Telescopes and radiometers. 3 Radio Telescopes and Radiometers Essential Radio Astronomy. (n.d.). Retrieved November 23, 2021, from <https://www.cv.nrao.edu/sransom/web/Ch3.html>.
- [9] "SPACETRACK REPORT NO. 3: Models for Propagation of NORAD Element Sets", December,31 1988, <https://celestrak.com/NORAD/documentation/spacetrk.pdf>
- [10] "Information Regarding Power Flux Density, Revision 2", 2016-07-22, <https://fcc.report/ELS/Space-Exploration-Technologies-Corp/0356-EX-PL-2015>
- [11] Peter Szabó and Katarína Gombíková (2019). Keplerian Orbit (<https://www.mathworks.com/matlabcentral/fileexchange/72098>) MATLAB Central File Exchange., Retrieved November 23, 2021.
- [12] "Chetvorno, CC0, via Wikimedia Commons", https://commons.wikimedia.org/wiki/File:Dipole_receiving_antenna.svg. Retrieved November 23, 2021.
- [13] "The Effects of Earth's Upper Atmosphere on Radio Signals", <https://radiojove.gsfc.nasa.gov/education/activities/iono.html>, Retrieved November 23, 2021.